Journal of Environmental Engineering and Energy

www.jeee.reapress.com

J. Environ. Eng. Energy.Vol. 1, No. 1 (2024) 47–58.

Paper Type: Original Article

Evaluation of Ammonia as a Replacement for Water in Surface Condensers: Performance and Efficiency

Hasan Hosseini[1], Asma Mozaffari[1], Zahra Khodabandeh[1,*], Seyed Mahmood Kia[1]

[1] Faculty of Mechanical and Energy Engineering, Shahid Beheshti University, Tehran, Iran; Hs.hoseini24@gmail.com; a.mozefferi@mail.sbu.ac.ir; zahra.khdbndh@gmail.com; mahmoud.kia.73@gmail.com.

Citation:

Received: 17 September 2024 *Revised: 16 November 2024* *Accepted:01 December 2024*	Hosseini, H., Mozaffari, A., Khodabandeh, Z., & Kia, S. M. (2024). Evaluation of ammonia as a replacement for water in surface condensers: performance and efficiency. *Journal of environmental engineering and energy*, *1* (1), 47-58.

Abstract

The present paper explores the possibility of replacing the water cooling stream with an ammonia stream in surface condensers. Considering the high enthalpy of phase change of ammonia, if the boiling process of ammonia replaces the water cooling process, then the required cooling for condensation can be provided at a smaller surface area and coolant flow rate. To this end, first, the ammonia flow in one tube of a sample surface condenser is modeled, and the heat transfer equations are solved for different inlet temperatures and flow rates. By repeating the solution with the tube length considered constant, the required inlet flow rate for one tube at different temperatures is obtained. Then, it computes the heat transferred from one tube, and by dividing the total heat needed for condensation of steam by the calculated heat, it obtains a relation for computing the total surface and flow rate required. The investigation results reveal that the ammonia flow rate required is considerably lower than that of water, and also, at low ammonia temperatures, the surface area required will be considerably low.

Keywords: Alternative fluid, Condenser, Ammonia, Coolant, Surface, Flow rate, Phase change.

1 | Introduction

Steam surface condensers are now very important parts of industries and, particularly, steam power plants, where circulating cooler water through condenser tubes ensures steam condensation on the shell side of the heat exchanger. Improvement in heat transfer efficiency can be achieved by the use of nanofluids, changes in flow patterns, changes in the flow regime, and pipe geometry. Meanwhile, nanofluids with high thermal conductivity combined with optimized flow designs and turbulators can significantly improve heat transfer rates [1–3]. All the improvement in flow patterns and fluid mixing contributes to enhancing the system performance, reducing the consumption of fossil fuel, and mitigating CO2 emission. Many studies have already validated these strategies in the thermal management system [4–8].

Corresponding Author: zahra.khdbndh@gmail.com

Many researchers have worked on optimizing condensers, and most of them are based on physical design parameters like tube arrangement, shape, and diameter. Mori et al. [9] optimized the heat transfer surface geometry to minimize the thickness of the condensed water layer on the tubes. Rabas [10] did a study replacing smooth tubes with rough and grooved tubes in the condenser to improve heat transfer. Zheng et al. [11] conducted numerical analyses of different tube configurations in the condenser to determine the optimum design. Yao et al. [12] investigated the effect of fin spacing on the enhancement of the performance of finned tube condensers. Zubair et al. [13] optimized two-phase heat exchangers using the second law of thermodynamics. Also, Mehrpooya et al. [14] proposed a combined power and refrigeration cycle with ammonia absorption and a solid oxide fuel cell. Although they investigated a mixture of water and ammonia as the condenser coolant instead of pure water for their design, the performance of the condenser was not explored in detail since the main objectives of the study were different. This paper considers another parameter, the coolant, to optimize the dimension and performance of the condenser.

The mass flow rate of the water in power plant condensers is quite large. For a 250-MW cycle, this represents about 5000 to 7000 kg/s. Reducing significantly this mass flow rate would imply considerable reductions in the sizing and losses of many components, such as piping, pumps, and the condenser itself. This is possible if we replace water with a fluid with a higher heat absorption capacity. It is because ammonia has a much higher enthalpy of vaporization than the enthalpy of temperature change of water; the cooling that is needed in the condenser tubes can be accomplished with a lower flow of ammonia since evaporating ammonia will give the required cooling.

Moreover, ammonia has much higher heat transfer coefficients in two-phase conditions than water [9], so the steam condensation may also need less area compared to water-cooled systems. To check the feasibility of this replacement, the surface condenser of the power plant panel is taken as a case study. Therefore, modeling of the heat transfer of the ammonia flow in a condenser tube is considered. It is assumed that ammonia enters as a saturated liquid, evaporates completely, and exits the tube as a saturated vapor (*Fig. 1*).

Modeling is carried out for a range of inlet temperatures and flow rates. For a given tube length, and assuming that ammonia is completely evaporated inside the tube, the heat transfer equation can be solved iteratively for a range of inlet temperatures to give the optimum inlet flow rate at each temperature. Knowing the total heat capacity, which the condenser requires, together with the heat capacity of the tube, its necessary flow rate and total surface area can be found [15].

Another main direction apart from condenser performance optimization is the integration of ammonia as a working fluid in such systems as Ocean Thermal Energy Conversion (OTEC). The characteristics of ocean thermal energy, as a clean energy source, offer several advantages, including large storage capacity and low pollution output [14], [16].

The OTEC system can be classified into open, closed, and hybrid cycles [17]. Among all cycles, the closed one—rankine-driven—is the most applied due to its ease in miniaturization [18]. Nevertheless, a small temperature difference between surface and deep seawater makes it difficult to improve the system efficiency [19]. Some enhancement methods have been presented by researchers, including the integration of solar energy [20] to deal with such a heat source, as well as the optimization of the working fluid. Indeed, among other refrigerants, ammonia (R717) shows a relatively high promising thermal efficiency [21]. Ejectors are considered essential elements in the enhancement of the efficiency level of the OTEC systems. The mechanism of an ejector relies on energy conversion associated with a high-pressure jet flow throughout the absorption and regeneration process of a system [22]. The efficiency of an ejector depends on working pressures and geometrical configurations [23], [24]. Previous research has demonstrated that optimization of these parameters could lead to great improvement in system efficiency [24]. The integration of ammonia as a working fluid in steam surface condensers and OTEC systems gives one of the most promising ways of improving performance. These unique thermal properties of ammonia combined with developments in ejector technology and exploration of alternative cooling fluids provide significant potential for improving energy efficiency in industrial applications [17].

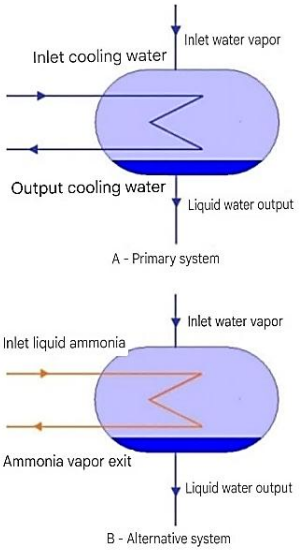

Fig. 1. Schematic diagram of the condenser in the initial state (A) and with ammonia replacing the cooling water (B).

In this work, heat transfer modeling is conducted based on different inlet temperatures and flow rates, which assume the complete evaporation of ammonia inside the condenser tube. This is solved using an iterative method where the solution for the heat transfer equation is obtained for each case, giving the highest flow rate and best inlet temperature. Based on the total heat capacity required by the system and the thermal capacity of the tubes, calculations are performed to achieve the right flow rate and surface area in optimizing the condenser performance.

2|Case Study: Surface Condenser Model and Specifications

The surface steam condenser of a power plant is used as an example of the ammonia flow replacement. The specifications and operation conditions of this condenser are shown in *Table 1*. This ammonia flow has to provide the entire thermal power required by this condenser.

Table 1. Technical specs and operating conditions of the steam cycle surface condenser.

S/N	Component	Specification
1	Heat duty	212737 Kw
2	Overall heat transfer area	7841 m2
3	Cooling water flow rate	5674 kg/s
4	Number of tubes	10748
5	Tube material	Stainless Steel
6	Diameter of tube	25.4 mm
7	Tube length	9.2 m
8	Tube thickness	2 mm

3|Heat Transfer Modeling of Ammonia Flow

The beginning: modeling of the cooling process by ammonia in one of the condenser tubes, calculation of heat transfer capacity in each tube. Dividing the total required heat capacity by the heat capacity of one tube gives the number of tubes. Unknowns in this section are the inlet velocity, temperature, pressure, and steam quality of ammonia at the tube's inlet. The physical dimensions of the tube (length, diameter, thickness, material) and the thermodynamic conditions of the condensing water vapor on the tube's surface are known parameters.

Assuming the intent of the problem is to utilize the enthalpy of phase change of ammonia [18], it is assumed that the ammonia enters the tube saturated with a steam quality of $x = 0$ and leaves the tube with a steam quality of $x = 1$.

Due to a large number of unknown parameters, it will take a long time to optimize, so we suggest the following procedure: by iteration and analyzing the variations of key parameters, such as the inlet velocity, the parameters are optimized.

Step 1. The inlet saturated temperature of ammonia and an initial assumed velocity for it are considered.

Step 2. Knowing the value of inlet velocity, together with that of the density of saturated liquid ammonia (ρ_f), and the internal diameter of the tube itself (D_i), it was possible to calculate the mass flow rate in the tube using *Eq. (1)* [19].

$$\dot{m} = \rho_f V_{in} D_i. \quad (1)$$

By calculating the mass flow rate and having the enthalpy of the phase change of ammonia at a given saturation temperature (h_{fg}), the needed heat capacity for complete evaporation of the ammonia in the pipe ($\dot{q}$) is estimated from *Eq. (2)* [20].

$$\dot{q} = \dot{m}\, h_{fg}. \quad (2)$$

Step 3. Having specified the mass flow rate and the heat to be removed, the evaporation process within the tube has to be modeled. To this end, the tube is subdivided into 50 elements of unknown length, cf. *Fig. 2*. The underlying principle of this partitioning is that in each section, the steam quality rises by 0.02.

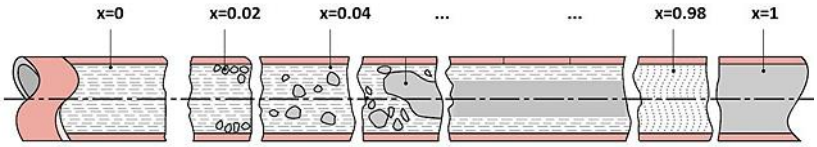

Fig. 2. Schematic representation of a tube element for modeling ammonia evaporation.

Step 4. The average steam quality at the inlet and outlet of each element is assumed to be the steam quality of that element. Hence, the qualities of the sections are defined to be a vector: X=[0.01,0.03,0.05,…,0.99].

Step 5. The parameter is defined as the required heat capacity per element in the shape of *Eq. (3)*, where N represents the number of tube elements. For each element, the heat transfer *Eq. (4)* is solved, and the surface area required is calculated [21].

$$\dot{q}_i = \dot{q}/n_x. \quad (3)$$

$$\dot{q}_i = U_i A_i \Delta T_i. \quad (4)$$

$$1/U_i = 1/h_w + r_{in} \ln(r_{out}/r_{in})/k_s + 1/h_{ai}. \quad (5)$$

In *Eq. (5)*, h_w is the heat transfer coefficient for water undergoing condensation, k_s is the thermal conductivity, r_{in} and r_{out} are the internal and external diameters of the steel tube, respectively, and h_ai is the heat transfer coefficient for ammonia vaporizing in each element. The value of k_s is 16, taken from the thermodynamic tables for stainless steel at 48°C, which is the condensation temperature of the vapor. The values of hw and hai are evaluated with the help of *Eq. (6)* and *Eq. (11)*, respectively.

$$h_w = 0.729\left[g\rho_1(\rho_1 - \rho_v)k_1^3\, h'_{fgw}/(N_o \mu_1 (T_{sat} - T_s) D_o)\right], \quad (6)$$

where in *Eq. (6)*, ρ_1, ρ_v, k_1, and μ_1, respectively, are the steam density, liquid density, heat transfer coefficient, and dynamic viscosity for the liquid at the saturation temperature; g is the gravitational constant, and D_o is the outer diameter of the pipe.

Now, the saturation temperature, T_{sat}, of the water and the temperature, T_s, at the pipe's surface are considered; this is roughly equal to the temperature of the fluid within the pipe.

Because steam directly hits the upper pipes and, by decreasing their quality, is condensed. Thus, moving downward, the quality of the liquid decreases. Hence, going downward, the lower pipes have more condensed liquid. With increasing liquid inventory on the lower tubes, the greater the heat transfer rate is reduced; in the above formula, it is necessary to reduce the parameter N_o to account for this effect. The number of vertical pipes is double the number of horizontal pipes. With this, in the final stage of the design, the number of tubes required can be found, with the condition being that the 30% margin is required by iteratively applying the specified parameter to find the exact number of tubes needed. The final formula for h'_{fgw} is given in *Eq. (7)* [22].

$$h'_{fgw} = h_{fgw}\left(1 + 0.68\, C_{pl}\right) Ja, \quad (7)$$

$$Ja = \left(C_{pl}(T_{sat} - T_s)\right) / h_{fgw}, \quad (8)$$

where in *Eq. (8),* C_{pi} is the heat capacity of saturated liquid water at a specified temperature, h_{fgw} is the enthalpy of the phase change of water, and Ja is the Jakob number.

Estimation of the convective heat transfer coefficient for ammonia is based on the available correlations for forced convective boiling heat transfer in a tube.

$$h_1/h_{sp} = 0.6683(\rho_1/\rho_v)^{0.1} \quad \overline{X}^{0.16}(1-\bar{x})^{0.64} f(Fr) + 1058(\dot{q}_s'/(G\, h_{fg}))^{0.7}(1-\bar{x})^{0.8} G_{s,f}. \quad (9)$$

$$h_2/h_{sp} = 1.136(\rho_1/\rho_v)^{0.45}\bar{x}^{0.72}(1-\bar{x})^{0.08} f(F_r) + 667 \cdot 2\left(\dot{q}'/\left(Gh_{fg}\right)\right)^{0.7}(1-\bar{x})^{0.8} G_{s,f}. \quad (10)$$

$$h_a = \max(h_1, h_2). \quad (11)$$

In these equations, $h_{sp}$is the convective heat transfer coefficient in the case where the entire pipe flow is considered to be in a saturated liquid phase [23]. This parameter can be calculated from *Eq. (12).*

$$h_{sp} = 0.023 Re_1^{0.8} Pr_1^{0.4} k_1/D_i. \quad (12)$$

$$Re = VD/\vartheta. \quad (13)$$

In *Eq. (12)*, Re_1, Pr_1 and k_1 represent the Reynolds number, the Prandtl number, and the fluid thermal conductivity in a saturated liquid state, respectively. D_i is the inner diameter of the pipe, ϑ is the kinematic viscosity. $\bar{x}$ is the average quality along the pipe, which, in this case, is taken equal to $\bar{x}$ for each section. The variable $\dot{q}'_s$ denotes the heat flux per unit area of the pipe. In order to find this flux, the total thermal power of the pipe $\ddot{q}$ may be divided by the total surface area of a pipe according to *Eq. (14).* In this relation, L is the length of a condenser pipe, and D_o is the outer diameter of the pipe.

$$\dot{q}'_s = \dot{q}/(\pi D_o L). \quad (14)$$

G is the mass flow rate per unit cross-sectional area of the pipe, which is a value obtained by dividing $\dot{m}$ by the cross-sectional area of the pipe. The Froude number (Fr) in these equations on the liquid phase is obtained from *Eq. (14).*

If $Fr \geq 0.04$, then the value of the function; otherwise, it is equal to $2.63Fr^{0.3}$. The coefficient $G_{s,f}$ depends on the material of the solid surface and the type of liquid, and for steel pipes, this value is considered to be 1. All the parameters provided can be calculated either through the equations given or from thermodynamic tables of water and ammonia. With all the parameters of *Eq. (5)* known, the value of (U_i) for each element can be obtained.

Step 6. The value of ΔT_i in *Eq. (4)* is equal to the temperature difference between the condensing water and the saturated ammonia. With U_i and $\dot{q}_i$ known for each element and substituting them into *Eq. (4)*, the surface area required for each element to raise the steam quality to the desired amount (A_i) is obtained.

Dividing this area by the perimeter of the pipe will give the length of each element L_i. Repeating this solution for each element will give the length of each element; then, the total length required, (L_{out}), will equal the sum of these lengths.

$$L_{tot} = \sum L_i. \quad (15)$$

Note that this length is gained based on the assumed inlet velocity and considering that the outlet steam quality will be equal to 1. The obtained length is compared with the length of the surface condenser pipe (L).

- *If $L_{out} > L$, the inlet flow rate is reduced by decreasing the velocity, and the solution is repeated.*
- *If $L_{out} < L$, the inlet flow rate is increased by raising the velocity, and the solution is repeated. This process continues until $L = L_{out}$.*

At this stage, the number of required pipes (N) can be determined by dividing the total heat transfer capacity ($\dot{q}_{tot} = 212737$) by the heat capacity of a single pipe.

$$\dot{q}'_s = \dot{q}/(\pi D_\circ L). \quad (16)$$

$$N = \dot{q}_{tot}/\dot{q}. \quad (17)$$

Additionally, the total required ammonia flow rate ($\dot{M}$) is obtained as follows:

$$M = N\dot{m}. \quad (18)$$

It can be more accurately calculated by determining the number of pipes and assuming a square arrangement. In this assumption, where the arrangement of pipes in a vertical array (*Fig. 3*) in the simplest case yields the same number as the square of the number obtained, changing the assumption from linear square arrangement to octagonal arrangement (as depicted in *Fig. 3*) results in the reduction of the obtained N_o by half.

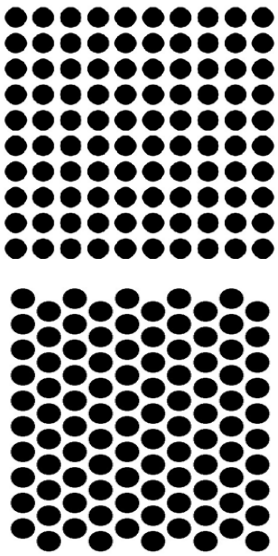

Fig. 3. Variations in the number of tubes and flow rate with increasing temperature and decreasing inlet.

After calculating N_o, this value is again put back into *Eq. (6)* and the solution is again repeated with more accuracy, and finally, an optimal inlet velocity at a given temperature is arrived at. Likewise, by changing the temperature and the inlet saturation conditions, the process may be repeated to evaluate the performances under different inlet temperature conditions.

4|Optimization of Heat Transfer and Flow Rate

To estimate the surface area saving, the parameter of surface-saving percentage (Sd) is defined based on *Eq. (19)*. The numerator is the saving in surface area compared with the water-cooled case, while the denominator is the surface area needed in the water-cooled case.

$$Sd = (A_{water} - A_{ammonia})/A_{water} \times 100. \quad (19)$$

Similarly, in order to quantify the saved flow, the parameter of flow-saving percentage (Md) is defined based on *Eq. (20)* [24]. The numerator is the saved cooling fluid flow compared with the water-cooled case, while the denominator is the required flow for the water-cooled case.

$$\mathrm{Md} = (\mathrm{M_{water}} - \mathrm{M_{ammonia}})/\mathrm{M_{water}} \times 100. \quad \textbf{(20)}$$

All processes and equations are coded and iterated in MATLAB software [25].

5 | Results and Discussion

First, the solution was run again at inlet temperatures of 25°C, 30°C, and 35°C. The trend of variations in $\mathrm{h_a}$ along the pipe length, and the rise in steam quality is depicted in *Fig. 4*.

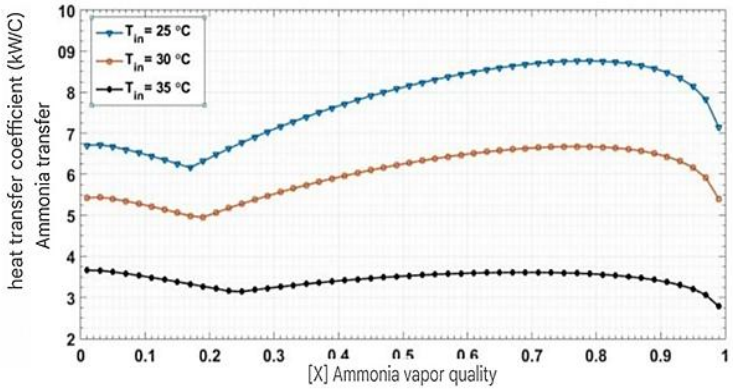

Fig. 4. Changes in h_a along the pipe with increasing steam quality at different temperatures.

Observations show that the heat transfer coefficient ($\mathrm{h_a}$)decreases with the increase of steam quality, starting from $\mathrm{x = 0}$ to $\mathrm{x = 0.2}$. However, as steam quality increases from $\mathrm{x = 0.2}$ to or $\mathrm{x = 0.85}$, ($\mathrm{h_a}$) increases significantly, and this increase strongly depends on the inlet temperature. Specifically, the lower the inlet ammonia temperature, the higher the value of ($\mathrm{h_a}$) and its growth rate along the pipe. After the steam quality exceeds $\mathrm{x = 0.8}$ $\mathrm{h_a}$ starts to decrease, and this downward trend continues until the end of the pipe. For a more detailed analysis, the calculations are repeated for the temperature range of 23°C to 33°C. The results of the average heat transfer coefficients along the length of the pipe ($\bar{\mathrm{U}}$ and $\bar{\mathrm{h}}_\mathrm{a}$) are presented in *Table 2*, and the results of the analysis of the surface and required flow rate are presented in *Table 3*.

Table 2. Changes in U¯ and h̄a with rising inlet temperature and variations in inlet.

Tin (˚C)	Vin (m/s)	ha (W/(m2˚C)	U(W/(m2˚C)
23	0.145	8454.35	1837.33
25	0.133	7751.68	1809.68
27	0.121	7035.61	1776.37
29	0.108	6296.89	1732.49
31	0.095	5580.89	1682.64
33	0.08	4529.21	1577.6

As can be seen from *Table 3*, the decrease in $\bar{\mathrm{h}}_\mathrm{a}$ cannot be explained by the temperature drop alone. However, when decreasing the inlet temperature, the inlet velocity of ammonia is decreased as well. According to *Eq. (12)* and *Eq. (13)*, this implies that a decrease in ammonia velocity leads to a decrease of the Reynolds number (Re) and, consecutively, in. The decrease in $\mathrm{h_{sp}}$ in *Eq. (9)* and *Eq. (10)* results in a reduction of $\mathrm{h_a}$. The variations of $\mathrm{h_a}$ with inlet velocity are plotted in *Fig. 5*.

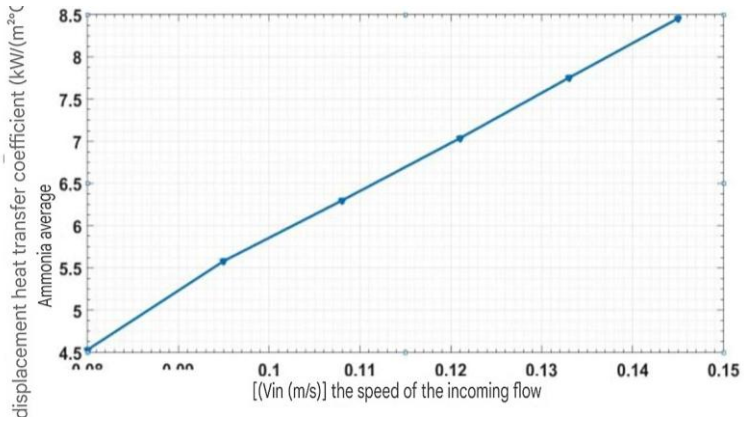

Fig. 5. Variations in $\bar{h}_a$, $\bar{U}$ with changes in the inlet velocity of ammonia.

Another important observation is that from *Table 2*, the big difference between $\bar{U}$ and $\bar{h}_a$. It would be expected that with such a high value from $\bar{h}_a$, $\bar{U}$ should also be bigger.

This discrepancy arises because in *Eq. (5)* is more sensitive than $\bar{U}$ to $\bar{h}_a$,. The h_w calculated values lie in the range of 3000-3500, which is invariably lower than $\bar{h}_a$. Therefore, the effect of from $\bar{U}$ from h_w is much higher compared to $\bar{h}_a$.

Table 3. Tube count and florate change with rising temperature and reduced inlet velocity.

Tin (°C)	N	M(kg/s)	Sd (%)	Md (%)
23	5685	181.26	47.11	96.81
25	6273	182.56	41.64	96.78
27	6981	183.89	35.05	96.76
29	7919	185.24	26.32	96.74
31	9118	186.65	15.17	96.71
33	10970	188.13	-2.07	96.68

It is found that, with the rise in inlet temperature of ammonia, the number of tubes required also increases. This trend is more clearly seen in *Fig. 6*. This increasing number of tubes can also be justified by the decrease in the inlet velocity. With the decrease in inlet velocity of the tubes, less mass is flowing through it. According to *Eq. (2)*, the mass flow rate of the tubes decreased, then the thermal power of the tube

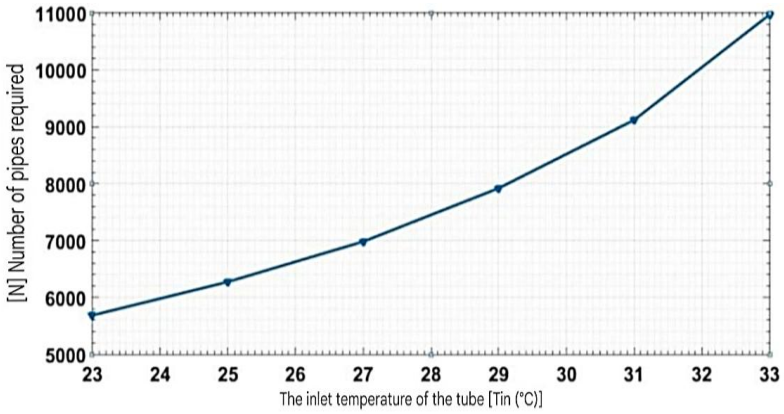

($\dot{q}$) decreases.

Fig. 6. Changes in N with increasing inlet temperature.

Assuming the total thermal power ($\dot{q}_{tot}$) remains constant in *Eq. (15)*, then the number of tubes (N) will increase. This increase in number is of such a nature that at higher temperatures it means more tubes are needed than the design limit and even results in more required surface area than that for water cooling; hence, a negative heat transfer surface savings coefficient.

Fig. 7 shows the sensitivity of and to an increase in the inlet temperature of ammonia. While the surface saving percentage is highly sensitive to the ammonia inlet temperature, percent mass flow savings stay almost insensitive w.r.t. changing inlet temperature.

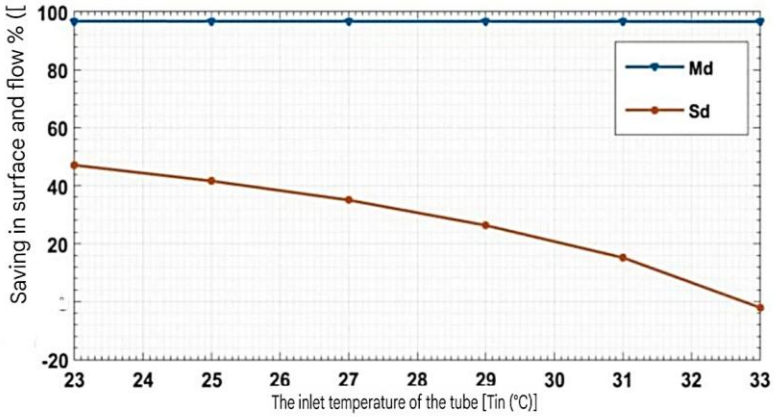

Fig. 7. Sensitivity of Md and Sd to changes in inlet temperature.

This is explained by the fact that assuming constant thermal power, the surface area required is bounded by the temperature difference times the overall heat transfer coefficient, as explained by *Eq. (4)*. The temperature difference is dependent on the inlet temperature, and the heat transfer coefficient itself is again a function of the inlet velocity. Therefore, the surface area required will vary with variations in the two parameters. Contrary to *Eq. (2)*, the mass flow rate required is now a function only of the enthalpy of phase change of ammonia, which indeed is independent of the inlet velocity and only slightly sensitive to rising temperature. More precisely, with increasing temperature, the enthalpy of phase change slightly decreases; hence - with constant total thermal power *Eq. (2)* to compensate for it.

6 | Conclusion

This means that the flow rate can be significantly reduced when boiling ammonia replaces steam heating in the condenser tubes. The calculations show that up to 96% of fluid flow can be saved. A reduction of this nature can dramatically reduce the size of piping, cooling pumps, and overall system losses. However, while the reduction in flow rate is relatively straightforward, the reduction in surface area is less so; it depends on specific temperature conditions. Increase in the temperature of the inlet ammonia, the temperature difference between the condensing steam decreases, reducing the heat transfer capacity for each tube.

When such is the case, then either the heat transfer surface area or the heat transfer coefficient has to be increased in order for compensation to be affected. Since it is the minimization of surface area that is the objective, attention would be on increasing the heat transfer coefficient. *Eqs. (6)-(11)* indicate that velocity is the most sensitive adjustable parameter influencing the factor of heat transfer coefficient. Hence, the overall heat transfer coefficient can be effectively increased by increasing the velocity.

However, as shown in *Eq. (2)*, an increase in the inlet velocity increases the mass flow rate of the saturated liquid and consequently raises the heat capacity of the tube. So, in *Eq. (4)* both the heat capacity as well as the heat transfer coefficient increase. Increasing the heat capacity of the tube is desirable since it would decrease the total number of tubes required to give the overall heat capacity requirement. This, however, is subject to the condition that complete evaporation of ammonia is achieved within the prescribed length of the tube. Otherwise, if the velocity is increased to infinity, then tube length would not be enough to have complete evaporation of ammonia.

Finally, assuming the target is to introduce ammonia into an existing surface condenser similar to the one studied in this paper, critical inlet temperature has to be estimated. For instance, for the power plant surface condenser with a turbine outlet steam temperature of 48°C, this critical temperature is about 32°C from *Table 2*. The reason is that if the inlet temperature is greater than this value, then the number of tubes required will

be higher than the actual number of tubes present in the condenser, and, therefore, the required heat capacity cannot be transferred. This replacement of ammonia is possible only if the inlet ammonia can be supplied at temperatures below or equal to the critical temperature. The lower the inlet temperature, the more surface area that can be saved. Even at an inlet temperature equal to the critical temperature—zero surface area savings—the high flow rate savings would still justify this replacement. However, it is important to note that replacement with a temperature higher than the critical temperature is not possible and certainly will disturb the performance of the condenser.

If one is interested in a new system and a new surface condenser, it is wise to use much longer tube lengths. As seen from *Fig. 4*, the ammonia heat transfer coefficient is very sensitive to inlet velocity. The longer the tube, the higher the heat transfer surface area for high-velocity two-phase ammonia, which, of course, has a higher heat transfer coefficient. In other words, a single long tube with a high velocity of ammonia can transfer more heat than multiple tubes having a combined length greater than the long tube but with a low flow velocity of ammonia. This is to say, higher ammonia inlet temperatures can be accommodated with careful and optimized design while at the same time providing substantial savings in surface area.

References

[1] Kia, S., Khanmohammadi, S., & Jahangiri, A. (2023). Experimental and numerical investigation on heat transfer and pressure drop of SiO2 and Al2O3 oil-based nanofluid characteristics through the different helical tubes under constant heat fluxes. *International journal of thermal sciences*, *185*, 108082. DOI:10.1016/j.ijthermalsci.2022.108082

[2] Kia, S. M., Nejati jahromi, M., & Isvand, H. (2022). Numerical simulation and experimental evaluation of an unsteady flow around forced rotating cylindrical prototype with three orthogonal plates. *Modares mechanical engineering*, *22*(11), 637-646. (**In Persian**). DOI:10.52547/mme.22.11.637

[3] Ashrafi, N., & Sadeghi, A. (2018). Numerical simulation of visco-plastic fluid flow between two parallel plates with triangular obstacles. *Bulletin of the American physical society*, *63*. https://meetings.aps.org/Meeting/DFD18/Event/334178

[4] Ashrafi, N., & Kia, S. M. (2018). Numerical simulation of an unsteady flow over a circular cylinder at high Reynolds numbers. *Bulletin of the American physical society*, *63*. https://meetings.aps.org/Meeting/DFD18/Session/D32.9

[5] Kia, S. M., & Talebi, F. (2018). Numerical investigation of unsteady flow around a circular cylinderat different reynolds number. *The 26th annual international conference of the Iranian society of mechanical engineers*, Semnan, Iran. Civilica. (**In Persian**). https://civilica.com/doc/1134380/

[6] Kia, S. M., Nobakhti, M. H., & Khayat, M. (2020). Experimental investigation on heat transfer and pressure drop of Al2O3-base oil nanofluid in a helically coiled tube and effect of turbulator on the thermal performance of shell and tube heat exchanger. *Journal of energy conversion*, *7*(3), 61-80. (**In Persian**). http://jeed.dezful.iau.ir/article-1-327-en.html

[7] Ikpe, A. E., Ekanem, I., & Ekanem, K. R. (2024). Conventional trends on carbon capture and storage in the 21st century: a framework for environmental sustainability. *Journal of environmental engineering and energy*, *1*(1), 1–15.

[8] Wilson, E. (2024). Temperature effects on the corrosion inhibition of mild steel in crude oil medium by methanolic extract of Persea Americana (Avocado tree). *Journal of environmental engineering and energy*, *1*(1), 16–23.

[9] Mori, Y., Hijikata, K., Hirasawa, S., & Nakayama, W. (1981). Optimized performance of condensers with outside condensing surfaces. *ASME journal of heat and mass transfer*, *103*(1), 96–102. https://doi.org/10.1115/1.3244439

[10] Rabas, T. J., & Schaefer, R. J. (1993). Evaluation of enhanced tubes for power plant condensers. *ASME journal of heat transfer*, *115*(2), 315–322.

[11] Zeng, H., Meng, J., & Li, Z. (2012). Numerical study of a power plant condenser tube arrangement. *Applied thermal engineering*, *40*, 294–303. DOI:10.1016/j.applthermaleng.2012.02.028

[12] Yau, K. K., Cooper, J. R., & Rose, J. W. (1985). Effect of fin spacing on the performance of horizontal integral-fin condenser tubes. *ASME journal of heat and mass transfer*, *107*(2), 377–386. https://doi.org/10.1115/1.3247425

[13] Zubair, S. M., Kadaba, P. V, & Evans, R. B. (1987). Second-law-based thermoeconomic optimization of two-phase heat exchangers. *ASME journal of heat and mass transfer*, *109*(2), 287–294. https://doi.org/10.1115/1.3248078

[14] Mehrpooya, M., Dehghani, H., & Ali Moosavian, S. M. (2016). Optimal design of solid oxide fuel cell, ammonia-water single effect absorption cycle and Rankine steam cycle hybrid system. *Journal of power sources*, *306*, 107–123. DOI:10.1016/j.jpowsour.2015.11.103

[15] Saedi, A., Jahangiri, A., Ameri, M., & Asadi, F. (2022). Feasibility study and 3E analysis of blowdown heat recovery in a combined cycle power plant for utilization in Organic Rankine Cycle and greenhouse heating. *Energy*, *260*, 125065. DOI:10.1016/j.energy.2022.125065

[16] Ubabuike, U. H., Ime, J. U., Anosike, A. C., & Wilson, E. O. (2024). Comparative performance study of kolanut biodiesel and conventional fossil diesel. *Journal of environmental engineering and energy*, *1*(1), 24–31.

[17] Khalil, M., Gunlazuardi, J., Ivandini, T. A., & Umar, A. (2019). Photocatalytic conversion of CO2 using earth-abundant catalysts: a review on mechanism and catalytic performance. *Renewable and sustainable energy reviews*, *113*, 109246. DOI:10.1016/j.rser.2019.109246

[18] Zhang, Y., Park, C., Kim, N. H., & Haftka, R. T. (2017). Function prediction at one inaccessible point using converging lines. *Journal of mechanical design*, *139*(5), 51402. DOI:10.1115/1.4036130

[19] Sreenath, S., Sudhakar, K., Yusop, A. F., Solomin, E., & Kirpichnikova, I. M. (2020). Solar PV energy system in Malaysian airport: glare analysis, general design and performance assessment. *Energy reports*, *6*, 698–712. DOI:10.1016/j.egyr.2020.03.015

[20] Sun, Y., Tang, B., Huang, W., Wang, S., Wang, Z., Wang, X., … & Tao, C. (2016). Preparation of graphene modified epoxy resin with high thermal conductivity by optimizing the morphology of filler. *Applied thermal engineering*, *103*, 892–900. DOI:10.1016/j.applthermaleng.2016.05.005

[21] Dammak, K., & El Hami, A. (2021). Thermal reliability-based design optimization using Kriging model of PCM based pin fin heat sink. *International journal of heat and mass transfer*, *166*, 120745. DOI:10.1016/j.ijheatmasstransfer.2020.120745

[22] Adebayo, T. S., Agyekum, E. B., Kamel, S., Zawbaa, H. M., & Altuntaş, M. (2022). Drivers of environmental degradation in Turkey: designing an SDG framework through advanced quantile approaches. *Energy reports*, *8*, 2008–2021. DOI:10.1016/j.egyr.2022.01.020

[23] Mohammad Rozali, N. E., Ho, W. S., Wan Alwi, S. R., Manan, Z. A., Klemeš, J. J., & Cheong, J. S. (2019). Probability-Power Pinch Analysis targeting approach for diesel/biodiesel plant integration into hybrid power systems. *Energy*, *187*, 115913. DOI:10.1016/j.energy.2019.115913

[24] Feldgun, V. R., & Yankelevsky, D. Z. (2020). The non-stationary dynamic analytical solution of a spherical/cylindrical cavity expansion. *Journal of applied mechanics, transactions asme*, *87*(11), 111006. DOI:10.1115/1.4048040

[25] Jahangiri, A., Ameri, M., Arshizadeh, S., & Alvari, Y. (2023). District heating and cooling for building energy flexibility. In *Building energy flexibility and demand management* (pp. 173–190). Elsevier. DOI: 10.1016/B978-0-323-99588-7.00008-0

[26] Arshizadeh, S., Khanmohammadi, S., Jahangiri, A., Sajedi, S. M. H., Panchal, H., Prakash, C., & Gupta, N. K. (2024). Thermodynamic modeling and multi-objective optimization of an operating double-effect absorption chiller driven by photovoltaic panel: a case study. *Journal of environmental engineering and energy*, *1*(1), 32–46. https://jeee.reapress.com/journal/article/view/22

[27] Alihosseini, N., Jahangiri, A., & Ameri, M. (2024). Energy, exergy, exergoeconomic, and exergoenvironmental analyses and multi-objective optimization of parallel two-stage compression on the domestic refrigerator-freezer. *International journal of air-conditioning and refrigeration*, *32*(1), 1–15. DOI:10.1007/s44189-024-00054-y

[28] Jahangiri, A., Ebrahim Sarbandi Farahani, M., Ahmadi, G., Shahsavar, A., Borzouei, A., & Gharehbaei, H. (2022). Coupled CFD and 3E (energy, exergy and economical) analysis of using windbreak walls in heller type cooling towers. *Journal of cleaner production*, *358*, 131550. DOI:10.1016/j.jclepro.2022.131550

[29] Mardan Dezfouli, A. H., Arshizadeh, S., Nikjah Bakhshayesh, M., Jahangiri, A., & Ahrari, S. (2024). The 4E emergy-based analysis of a novel multi-generation geothermal cycle using LNG cold energy recovery. *Renewable energy*, *223*, 120084. DOI:10.1016/j.renene.2024.120084

[30] Ahmadi, G., Jahangiri, A., & Toghraie, D. (2023). Design of heat recovery steam generator (HRSG) and selection of gas turbine based on energy, exergy, exergoeconomic, and exergo-environmental prospects. *Process safety and environmental protection*, *172*, 353–368. DOI:10.1016/j.psep.2023.02.025

[31] Hosseinizadeh, S. E., Majidi, S., Goharkhah, M., & Jahangiri, A. (2021). Energy and exergy analysis of ferrofluid flow in a triple tube heat exchanger under the influence of an external magnetic field. *Thermal science and engineering progress*, *25*, 101019. DOI:10.1016/j.tsep.2021.101019

[32] Jahangiri, A., Yahyaabadi, M. M., & Sharif, A. (2019). Exergy and economic analysis of using the flue gas injection system of a combined cycle power plant into the Heller Tower to improve the power plant performance. *Journal of cleaner production*, *233*, 695–710. DOI:10.1016/j.jclepro.2019.06.077

[33] Shahsavar, A., Jahangiri, A., Qatarani nejad, A., Ahmadi, G., & Karamzadeh dizaji, A. (2022). Energy and exergy analysis and multi-objective optimization of using combined vortex tube-photovoltaic/thermal system in city gate stations. *Renewable energy*, *196*, 1017–1028. DOI:10.1016/j.renene.2022.07.057